



This discussion paper is/has been under review for the journal Atmospheric Measurement Techniques (AMT). Please refer to the corresponding final paper in AMT if available.

A six-beam method to measure turbulence statistics using ground-based wind lidars

A. Sathe, J. Mann, N. Vasiljevic, and G. Lea

DTU Wind Energy, Risø campus, Roskilde, Denmark

Received: 22 September 2014 – Accepted: 29 September 2014 – Published: 10 October 2014

Correspondence to: A. Sathe (amsat@dtu.dk)

Published by Copernicus Publications on behalf of the European Geosciences Union.

Six-beam method

A. Sathe et al.

Title Page

Abstract

Introduction

Conclusions

References

Tables

Figures



Back

Close

Full Screen / Esc

Printer-friendly Version

Interactive Discussion



Abstract

A so-called six-beam method is proposed to measure atmospheric turbulence using a ground-based wind lidar. This method requires measurement of the radial velocity variances at five equally spaced azimuth angles on the base of a scanning cone and one measurement at the center of the scanning circle, i.e. using a vertical beam at the same height. The scanning configuration is optimized to minimize the sum of the random errors in the measurement of the second-order moments of the components (u, v, w) of the wind field. We present this method as an alternative to the so-called velocity azimuth display (VAD) method that is routinely used in commercial wind lidars, and which usually results in significant averaging effects of measured turbulence. In the VAD method, the high frequency radial velocity measurements are used instead of their variances. The measurements are performed using a pulsed lidar (WindScanner), and the derived turbulence statistics (using both methods) such as the u and v variances are compared with those obtained from a reference cup anemometer and a wind vane at 89 m height under different atmospheric stabilities. The measurements show that in comparison to the reference cup anemometer, depending on the atmospheric stability and the wind field component, the six-beam method measures between 85–101 % of the reference turbulence, whereas the VAD method measures between 66–87 % of the reference turbulence.

1 Introduction

Wind lidars are being used significantly for wind energy applications. They measure mean wind speeds with great accuracy, and are very useful tools in the measurement of wind profiles (Smith et al., 2006; Kindler et al., 2007; Peña et al., 2009; Wagner et al., 2011). New recommended practices are being defined for wind resource assessments (Clifton et al., 2013). However their use in measuring atmospheric turbulence has not yet been established, particularly with the commercial lidars (Sathe et al., 2011b). The

Six-beam method

A. Sathe et al.

Title Page

Abstract

Introduction

Conclusions

References

Tables

Figures



Back

Close

Full Screen / Esc

Printer-friendly Version

Interactive Discussion



Six-beam method

A. Sathe et al.

Title Page

Abstract

Introduction

Conclusions

References

Tables

Figures



Back

Close

Full Screen / Esc

Printer-friendly Version

Interactive Discussion



main reason is that for a commercial lidar, the measured lidar data is processed using the so-called velocity azimuth display (VAD) method, where the measurements of the radial velocity (also called as the line-of-sight velocity) at different azimuth angles are combined to deduce the wind field components. For the mean wind speed estimation, the VAD method produces negligible errors. For turbulence statistics the VAD method produces significant systematic errors (Sathe et al., 2011b; Sathe and Mann, 2012) mainly due to two reasons; one is the filtering of the smaller scales due to the large size of the probe volume within which the radial velocity is measured, and second is the contamination by the two-point correlation between the components of the wind field.

In this article we present a so-called six-beam method that significantly improves the measurement of turbulence in comparison to the VAD method. This method uses the variances of the radial velocities from six different lidar beams, five of which are at equally spaced azimuth angles on the base of a scanning cone and one beam is vertical. These variances are then combined in order to deduce the second-order moments of the wind field. A framework for this method was originally proposed by Lhermitte (1969), which was used by Wilson (1970); Kropfli (1986) for radar studies, and subsequently by Eberhard et al. (1989); Mann et al. (2010) for lidar studies of turbulence measurements. In their studies only the covariances were estimated, either by combining several measurements of the radial velocity variances from several lidar beams (Eberhard et al., 1989) at equally spaced azimuth angles and one elevation angle, or by using only two lidar beams (Mann et al., 2010). In the present work, six beams are used, five at an elevation angle of 45° and one vertical that enable us to also deduce the variances.

The ideas to measure turbulence using remote sensing instruments have evolved, albeit slowly, since the pioneering works on radar meteorology (Lhermitte, 1962; Browning and Wexler, 1968). Based on the VAD scanning, Lhermitte (1969) was the first (to our knowledge) to suggest a technique of deducing turbulence using the measurements of the variance of the radial velocity. Subsequently Wilson (1970) was the first to conduct an experiment using a pulsed Doppler radar and deducing turbulence

Six-beam method

A. Sathe et al.

Title Page

Abstract

Introduction

Conclusions

References

Tables

Figures



Back

Close

Full Screen / Esc

Printer-friendly Version

Interactive Discussion



in the convective boundary layer (0.1–1.3 km). Only turbulence scales larger than the pulse volume but smaller than the scanning circle could be measured since all the data from a single scan was used. Also, no comparison with any reference instrument was carried out, and hence, the reliability of the radar measurements could not be verified. Kropfli (1986) extended the study of Wilson (1970) to also include the turbulence scales larger than the scanning circle by using the data from multiple scans. Although the method was developed for Doppler radar studies, it could also be used for Doppler lidar studies. Eberhard et al. (1989) was the first to perform turbulence studies using a lidar following the methods of Wilson (1970); Kropfli (1986). Gal-Chen et al. (1992) also used the variances of the radial velocities to deduce turbulence, but with a different scanning configuration. In all of the aforementioned studies with a Doppler lidar (or radar), the probe length was quite significant (of the order of 100 m), which perhaps was the reason to restrict these studies to the convective boundary layer. However if the turbulence measurements were desired close to the ground then they would be subjected to a significant amount of probe volume averaging. It was perhaps this reason that the focus on turbulence research with lidars shifted to understanding the probe volume averaging effect and providing potential solutions to compensate for it (Frehlich, 1994, 1997; Frehlich et al., 1994, 1998, 2006, 2008; Frehlich and Cornman, 2002; Frehlich and Kelley, 2008; Banakh et al., 1995a, b, 1996, 1999, 2010; Banakh and Smalikho, 1997a, b; Banakh and Werner, 2005; Smalikho, 1995; Smalikho et al., 2005; Mann et al., 2010; Branlard et al., 2013). Even with the development of the modern lidar systems, where the probe lengths have shrunk to about 30 m for a pulsed lidar, significant amount of averaging still remains in the turbulence measurements within the surface layer, where the wind turbines operate (Mann et al., 2009, 2010; Sjöholm et al., 2009; Sathe et al., 2011b; Sathe and Mann, 2012). A detailed review of the state of the art with respect to turbulence measurements using ground-based wind lidars can be found in Sathe and Mann (2013).

Unfortunately within the wind energy sector, turbulence measurements are being deduced using the VAD scanning method, which results in a significant amount of filtering

Six-beam method

A. Sathe et al.

Title Page

Abstract

Introduction

Conclusions

References

Tables

Figures

◀

▶

◀

▶

Back

Close

Full Screen / Esc

Printer-friendly Version

Interactive Discussion



of turbulence, and contamination by the two-point correlation between the components of the wind field (Sathe et al., 2011b). In this work we attempt to significantly improve the turbulence measurements compared to those obtained by the VAD method, by extending the previously developed ideas of using the radial velocity variances (Lhermitte, 1969; Wilson, 1970; Kropfli, 1986; Eberhard et al., 1989; Mann et al., 2010), but restricting them to using only six beams.

The structure of this article is divided into the following sections. Section 2 gives a detailed explanation of the six-beam technique. The optimum six-beam configuration, which is one of the main contributions of this article is also described in detail. In order to verify our method, turbulence measurements using a pulsed lidar windscanner were performed and compared them with a reference cup anemometer at a height of 89 m. The site description for the measurements is given in Sect. 3, whereas the results are described in Sect. 4. Discussions and conclusions are made in Sects. 5 and 6, respectively.

2 Theory of six-beam configuration

The instantaneous velocity field is characterized as a vector $\mathbf{v} = (u, v, w)$, and turbulence is characterized as the components of the Reynolds stress tensor,

$$\mathbf{R} = \begin{bmatrix} \langle u'^2 \rangle & \langle u'v' \rangle & \langle u'w' \rangle \\ \langle v'u' \rangle & \langle v'^2 \rangle & \langle v'w' \rangle \\ \langle w'u' \rangle & \langle w'v' \rangle & \langle w'^2 \rangle \end{bmatrix}, \quad (1)$$

where the diagonal terms are the variances of the respective wind field components and the off-diagonal terms are the covariances, $\langle \rangle$ denote ensemble average, and $'$ denotes fluctuations around the average.

As shown in Fig. 1, at a given instant of time if we assume that a lidar measures at a point, and that the lidar beam is inclined at a certain zenith angle ϕ (in some

literature the complement of ϕ is used, which is called as the elevation angle $\alpha = 90^\circ - \phi$ from the vertical axis, and makes an azimuth angle θ with respect to the axes in the horizontal plane, then the radial velocity (also called as the line-of-sight velocity) can be mathematically written as,

$$v_r(\phi, \theta, d_f) = \mathbf{n}(\phi, \theta) \cdot \mathbf{v}(\mathbf{n}(\phi, \theta)d_f), \quad (2)$$

where v_r is the radial velocity measured at a point, $\mathbf{n} = (\cos\theta \sin\phi, \sin\theta \sin\phi, \cos\phi)$ is the unit directional vector for a given ϕ and θ , and d_f is the distance at which the measurement is obtained. In Eq. (2), we have implicitly assumed that v_r is positive for the wind going away from the lidar axis, the coordinate system is right-handed, and u is aligned with the x_1 axis in a horizontal plane, i.e. from west to east. In reality, a lidar never receives backscatter from exactly a point, but from all over the physical space. Fortunately the transverse dimensions of a lidar beam are much smaller than the longitudinal dimensional, and for all practical purposes we can consider that the backscatter is received only along the lidar beam axis. Mathematically the radial velocity can be represented as the convolved signal,

$$\tilde{v}_r(\phi, \theta, d_f) = \int_{-\infty}^{\infty} \varphi(s) \mathbf{n}(\phi, \theta) \cdot \mathbf{v}(\mathbf{n}(\phi, \theta)(d_f + s)) ds, \quad (3)$$

where \tilde{v}_r is the weighted average radial velocity, $\varphi(s)$ is any weighting function integrating to one that depends on the type of lidar, i.e. a continuous wave (c-w) lidar or a pulsed lidar, and s is the distance along the beam from the measurement point of interest. From simple geometrical considerations the radial velocity variance can be written as a function of the components of \mathbf{R} (Lhermitte, 1969; Eberhard et al., 1989),

$$\begin{aligned} \langle v_r'^2 \rangle &= \langle u'^2 \rangle \sin^2 \phi \cos^2 \theta + \langle v'^2 \rangle \sin^2 \phi \sin^2 \theta + \langle w'^2 \rangle \cos^2 \phi \\ &+ 2 \langle u'v' \rangle \sin^2 \phi \sin \theta \cos \theta + 2 \langle u'w' \rangle \sin \phi \cos \phi \cos \theta + 2 \langle v'w' \rangle \sin \phi \cos \phi \sin \theta, \end{aligned} \quad (4)$$

Six-beam method

A. Sathe et al.

Title Page

Abstract

Introduction

Conclusions

References

Tables

Figures

◀

▶

◀

▶

Back

Close

Full Screen / Esc

Printer-friendly Version

Interactive Discussion



where $\langle v_r'^2 \rangle$ is the radial velocity variance. From Eq. (4) we can see that for a given θ and ϕ , if we have six measurements of $\langle v_r'^2 \rangle$ then there are six unknowns to be determined, which in a matrix form can be written as,

$$\mathbf{M} \underbrace{\begin{bmatrix} \langle u'^2 \rangle \\ \langle v'^2 \rangle \\ \langle w'^2 \rangle \\ \langle u'v' \rangle \\ \langle u'w' \rangle \\ \langle v'w' \rangle \end{bmatrix}}_{\boldsymbol{\Sigma}} = \underbrace{\begin{bmatrix} \langle v_{r_1}'^2 \rangle \\ \langle v_{r_2}'^2 \rangle \\ \langle v_{r_3}'^2 \rangle \\ \langle v_{r_4}'^2 \rangle \\ \langle v_{r_5}'^2 \rangle \\ \langle v_{r_6}'^2 \rangle \end{bmatrix}}_{\mathbf{S}}, \quad (5)$$

where $\boldsymbol{\Sigma}$ is a vector of the components of \mathbf{R} (because \mathbf{R} is symmetric, we only need six components), \mathbf{M} is a 6×6 matrix of the coefficients of $\boldsymbol{\Sigma}$ that consist of different combinations of θ and ϕ (see Eq. 4), and \mathbf{S} is a vector of measurements of $\langle v_r'^2 \rangle$ at different θ and ϕ (where the suffices denote measurements from beam 1 to 6). In principle we can then estimate $\boldsymbol{\Sigma}$ using the relation $\boldsymbol{\Sigma} = \mathbf{M}^{-1}\mathbf{S}$, where $^{-1}$ denotes matrix inverse. It is interesting to know beforehand, whether the measurements from the six beams on only one zenith angle are adequate, i.e. whether we can have six θ s and only one ϕ .

From fundamental algebra we understand that Eq. (5) will have a finite solution if and only if $\det \mathbf{M} \neq 0$, where \det denotes the determinant of a matrix. In other words \mathbf{M} should not be a degenerate matrix. From the properties of determinants we know that if any two rows (or columns) of a matrix are identical then its determinant is zero. Also, if the elements of any row (or column) are increased (or decreased) by equal multiples of the corresponding elements of any other row (or column), the value of determinant is unchanged. If we use only one ϕ at different θ , and add the first two columns of \mathbf{M} , we

Six-beam method

A. Sathe et al.

Title Page

Abstract

Introduction

Conclusions

References

Tables

Figures

◀

▶

◀

▶

Back

Close

Full Screen / Esc

Printer-friendly Version

Interactive Discussion



get the first and the third columns of \mathbf{M} to be multiples of each other, which according to the property of determinants implies $\det \mathbf{M} = 0$. Thus \mathbf{M} becomes degenerate if we use only one ϕ , and thus need $\langle v_r'^2 \rangle$ measurements from more than one ϕ .

We are then confronted with the challenge of obtaining an optimum combination of θ and ϕ . Measured \mathbf{S} is stochastic, and the random error of $\mathbf{\Sigma}$ will depend on the particular choice of the θ s and ϕ s. We thus choose the objective function such that the sum of the random errors of the components of $\mathbf{\Sigma}$ are minimized. For simplicity, we neglect the probe volume filtering effect in the derivation of the optimum combination, but including that will not change the optimum configuration.

2.1 Formulation of the objective function

Equation (4) is valid for the mean wind direction aligned in the x_1 direction. Following standard meteorological conventions, let us consider the mean wind direction to be at an angle Θ with respect to the North, i.e. x_2 axis as shown in Fig. 2. At first we derive an objective function for the wind aligned with the x_1 axis, and then extend the derivation to the coordinate system aligned with the mean wind direction.

2.1.1 Mean wind aligned with the x_1 axis

If we consider that $\delta \mathbf{\Sigma}$ is the random error on $\mathbf{\Sigma}$, and $\delta \mathbf{S}$ is the random error on \mathbf{S} , then Eq. (5) can be written as,

$$\begin{aligned} \mathbf{M}(\mathbf{\Sigma} + \delta \mathbf{\Sigma}) &= \mathbf{S} + \delta \mathbf{S}, \\ \mathbf{\Sigma} + \delta \mathbf{\Sigma} &= \mathbf{M}^{-1}(\mathbf{S} + \delta \mathbf{S}). \end{aligned} \quad (6)$$

We can thus write,

$$\delta \mathbf{\Sigma} = \mathbf{M}^{-1} \delta \mathbf{S}. \quad (7)$$

If we consider the sum of the error variances $\langle \delta \mathbf{\Sigma}^T \delta \mathbf{\Sigma} \rangle$, where T denotes matrix transpose, then the objective is to minimize the sum of the error variances of the components

Title Page

Abstract

Introduction

Conclusions

References

Tables

Figures

◀

▶

◀

▶

Back

Close

Full Screen / Esc

Printer-friendly Version

Interactive Discussion



of Σ . Taking the transpose and multiplying by Eq. (7) we get,

$$\begin{aligned}\delta\Sigma \cdot \delta\Sigma &= \delta\Sigma^T \delta\Sigma = (\mathbf{M}^{-1} \delta\mathcal{S})^T (\mathbf{M}^{-1} \delta\mathcal{S}) \\ &= \delta\mathcal{S}^T (\mathbf{M}^{-1T} \mathbf{M}^{-1}) \delta\mathcal{S}\end{aligned}\quad (8)$$

- 5 The task now is to simplify Eq. (8) such that it can be represented as a function of θ and ϕ only. If we assume that the random errors in the variances of the radial velocities are independent of each other, and that the error variance for each radial velocity variance is $\langle \epsilon_s^2 \rangle$, we get,

$$\frac{\langle \delta\Sigma^T \delta\Sigma \rangle}{\langle \epsilon_s^2 \rangle} = \text{Tr}(\mathbf{M}^{-1} \mathbf{M}^{-1T}),\quad (9)$$

10 where Tr is the trace of a matrix. The objective function is to minimize Eq. (9).

2.1.2 Coordinate system aligned with the mean wind direction

In order to align the coordinate system with the mean wind direction, we need to apply coordinate transformations on any tensors that are defined in the original coordinate system. The vector \mathbf{v} rotated in the mean wind direction has to be multiplied by a transformation matrix \mathbf{T} given as,

$$\mathbf{T} = \begin{bmatrix} -\sin\Theta & -\cos\Theta & 0 \\ \cos\Theta & -\sin\Theta & 0 \\ 0 & 0 & 1 \end{bmatrix}.\quad (10)$$

20 In the coordinate system aligned with the mean wind direction, we then get in matrix form,

$$\mathbf{R}_r = \mathbf{TRT}^T,\quad (11)$$

where \mathbf{R}_r is the Reynolds stress tensor in a coordinate system aligned with the mean wind direction. If we denote Σ_r as the vector of the components of \mathbf{R}_r , then we can write,

$$\Sigma_r = \underbrace{\begin{bmatrix} \sin^2 \Theta & \cos^2 \Theta & 0 & \sin 2\Theta & 0 & 0 \\ \cos^2 \Theta & \sin^2 \Theta & 0 & -\sin 2\Theta & 0 & 0 \\ 0 & 0 & 1 & 0 & 0 & 0 \\ -\frac{1}{2} \sin 2\Theta & \frac{1}{2} \sin 2\Theta & 0 & -\cos 2\Theta & 0 & 0 \\ 0 & 0 & 0 & 0 & -\sin \Theta & -\cos \Theta \\ 0 & 0 & 0 & 0 & \cos \Theta & -\sin \Theta \end{bmatrix}}_{\mathbf{N}} \Sigma. \quad (12)$$

Using Eqs. (6) and (7), we can write,

$$\delta \Sigma_r = \mathbf{N} \mathbf{M}^{-1} \delta S \quad (13)$$

Following the same procedure as in Sect. 2.1.1, we get

$$\frac{\langle \delta \Sigma_r^T \delta \Sigma_r \rangle}{\langle \epsilon_s^2 \rangle} = \text{Tr}(\mathbf{N} \mathbf{M}^{-1} (\mathbf{N} \mathbf{M}^{-1})^T). \quad (14)$$

Equation (14) states that the error variance is dependent on the mean wind direction. In order to make it independent of the mean wind direction, we assume a uniform distribution of the mean wind direction, and estimate the averaged ratio of the error variance. Thus the directionally averaged ratio is,

Six-beam method

A. Sathe et al.

Title Page

Abstract

Introduction

Conclusions

References

Tables

Figures

◀

▶

◀

▶

Back

Close

Full Screen / Esc

Printer-friendly Version

Interactive Discussion



$$\begin{aligned} \frac{\overline{\langle \delta \Sigma_r^T \delta \Sigma_r \rangle}}{\langle \epsilon_s^2 \rangle} &= \frac{1}{2\pi} \int_0^{2\pi} \text{Tr}(\mathbf{NM}^{-1}(\mathbf{NM}^{-1})^T) d\Theta \\ &= \frac{1}{2\pi} \int_0^{2\pi} \text{Tr}(\mathbf{NM}^{-1} \mathbf{M}^{-1T} \mathbf{N}^T) d\Theta, \end{aligned}$$

where $\overline{\dots}^\Theta$ denotes directional average. Using the property of matrix trace that it is invariant under cyclic permutations we get,

$$\frac{\overline{\langle \delta \Sigma_r^T \delta \Sigma_r \rangle}}{\langle \epsilon_s^2 \rangle} = \frac{1}{2\pi} \int_0^{2\pi} \text{Tr}(\mathbf{N}^T \mathbf{NM}^{-1} \mathbf{M}^{-1T}) d\Theta \quad (15)$$

We can also switch the order between integration and matrix trace, i.e. either we can estimate the trace first and then the integration or vice-versa. Thus,

$$\frac{\overline{\langle \delta \Sigma_r^T \delta \Sigma_r \rangle}}{\langle \epsilon_s^2 \rangle} = \text{Tr} \left(\left[\frac{1}{2\pi} \int_0^{2\pi} \mathbf{N}^T \mathbf{N} d\Theta \right] \mathbf{M}^{-1} \mathbf{M}^{-1T} \right). \quad (16)$$

Solving the integral we get,

$$\frac{\overline{\langle \delta \Sigma_r^T \delta \Sigma_r \rangle}}{\langle \epsilon_s^2 \rangle} = \text{Tr} \left(\begin{bmatrix} \frac{7}{8} & \frac{1}{8} & 0 & 0 & 0 & 0 \\ \frac{1}{8} & \frac{7}{8} & 0 & 0 & 0 & 0 \\ 0 & 0 & 1 & 0 & 0 & 0 \\ 0 & 0 & 0 & \frac{3}{2} & 0 & 0 \\ 0 & 0 & 0 & 0 & 1 & 0 \\ 0 & 0 & 0 & 0 & 0 & 1 \end{bmatrix} \mathbf{M}^{-1} \mathbf{M}^{-1T} \right). \quad (17)$$

Six-beam method

A. Sathe et al.

Title Page	
Abstract	Introduction
Conclusions	References
Tables	Figures
◀	▶
◀	▶
Back	Close
Full Screen / Esc	
Printer-friendly Version	
Interactive Discussion	



Six-beam method

A. Sathe et al.

Title Page

Abstract

Introduction

Conclusions

References

Tables

Figures

◀

▶

◀

▶

Back

Close

Full Screen / Esc

Printer-friendly Version

Interactive Discussion



WindScanner is based on the pulsed lidar Windcube 200 from Leosphere and a dual-axis mirror based steerable scanner head designed by DTU Wind Energy and IPU. The WindScanner is intended for radial velocity measurements from the range of distances between 50 and 6000 m. The current maximum measurement rate is 10 Hz. The maximum number of simultaneous radial velocities acquired at any rate along each line-of-sight is 500. The WindScanner can emit either 400 or 200 ns laser pulses, which are streamed with two corresponding pulse repetition frequencies of 10 and 20 kHz respectively. The energy content of 400 ns laser pulses is 100 μJ , while the energy content of the 200 ns laser pulses is half of this value. The scanner head has two rotational degrees of freedom and can rotate around the azimuth and elevation axes, thus it directs the laser pulses into the atmosphere at any combination of azimuth and elevation. The maximum scanner head rotation speed is 50°s^{-1} , while the maximum acceleration is 100°s^{-2} . The scanner head can rotate around both axes from 0 to 360° , and the rotation can be endless. The pointing accuracy of the WindScanner is 0.05° . The WindScanner is operated via a remote “master computer” through a UDP/IP and TCP/IP network using the remote sensing communication protocol (RSComPro) (Vasiljevic, 2014).

The measurements were performed at the Danish National Test Center for Large Wind Turbines at Høvsøre, Denmark. Figure 3 shows the location of the test center in Denmark (see inset in Fig. 3) and the location of the reference 89 m meteorological (met) mast located at the UTM zone 32 V 447 229 m E and 6 256 195 m N (WGS84 datum). The high frequency measurements from a reference Risø P2564A cup anemometer at 89 m placed on the top of the met mast are combined with the wind direction measurements from a F2919A Vector W200P wind vane placed in the north direction at 86 m to deduce $\langle u'^2 \rangle$ and $\langle v'^2 \rangle$ over a 30 min period. Since it is not possible to measure the w component using a cup anemometer, comparisons of the corresponding second-order statistics were not possible with the WindScanner measurements. The choice of the 30 min averaging period (instead of the standard 10 min statistics prevalent in the wind energy industry) is made based on the considerations

Six-beam method

A. Sathe et al.

Title Page

Abstract

Introduction

Conclusions

References

Tables

Figures

◀

▶

◀

▶

Back

Close

Full Screen / Esc

Printer-friendly Version

Interactive Discussion



of the random errors in turbulence measurements (Lenschow et al., 1994). The site is about 2 km from the west coast of Denmark. The eastern sector is characterized by flat homogeneous terrain, and to the south is a lagoon. The WindScanner is placed at the UTM zone 32 V 447 188 m E and 6 256 189 m N (WGS84 datum) which is about 41 m away from the met mast in the west direction. Since the wind turbines are to the east of the WindScanner and the met mast, the measurements only from the western sector (225–315°) are used. Owing to the sudden change in the surface roughness from sea to land in the western sector, we expect the turbulence structure to be influenced by the development of the internal boundary layer, particularly under different atmospheric stabilities. However we do not expect a significant influence on the flow homogeneity in the horizontal direction around the scanning circle, which is one of the key assumptions of the six-beam method.

The duration of the full cycle of the six-beam measurements from the WindScanner was about 15 s. The period of measurement was between 1–28 July 2013, where 764 30 min periods were measured. After filtering for data availability within each 30 min period, where only those periods were chosen with 95 % data, the number of 30 min periods reduced to 625. Finally filtering for wind directions to avoid wakes from the wind turbines and the met mast rendered 401 30 min periods. The available 30 min ensembles are further classified into different atmospheric stabilities, characterized by Monin–Obukhov length L_{MO} based on the intervals given in Table 2 (Sathe et al., 2011a). L_{MO} is estimated using the eddy covariance method (Kaimal and Finnigan, 1994) from the high frequency (20 Hz) measurements of a sonic anemometer at 80 m, that is mounted on a 116 m tall met mast (UTM zone 32 V 447 647 m E and 6 255 435 m N WGS84 datum) in the south-east direction (see Fig. 3). Mathematically, L_{MO} is given as,

$$L_{MO} = -\frac{u_*^3 \overline{\theta_v}}{\kappa g w' \overline{\theta_v'}}, \quad (18)$$

where u_* is the friction velocity, $\kappa = 0.4$ is the von Kármán constant, g is the acceleration due to gravity, θ_v is the virtual potential temperature, $\overline{\quad}$ denotes time average,

and $\overline{w'\theta'_v}$ (covariance of w and θ_v) is the virtual kinematic heat flux. u_* is estimated as,

$$u_* = \sqrt[4]{\overline{u'w'}^2 + \overline{v'w'}^2}, \quad (19)$$

where $\overline{u'w'}$ (covariance of u and w) and $\overline{v'w'}$ (covariance of v and w) are the vertical fluxes of the horizontal momentum.

As an initial validation of the accuracy and precision of the WindScanner, the 30 min mean wind speeds were compared with those obtained from the cup anemometer. Figure 4 shows that the WindScanner is very accurate (within 0.1 %) and precise (coefficient of determination, $r^2 \approx 0.9993$) in measuring the mean wind speeds. For one 30 min period, the mean radial velocities measured by each of the six beams on the base of the scanning cone were fitted to Eq. (2) in a least squares sense to obtain the 30 min mean wind speed. This procedure was repeated for all 30 min periods. It is to be noted that the mean wind speed obtained using both methods (six-beam and VAD) is identical, since averaging the radial velocity for each beam, and then making a linear fit to obtain the u , v , and w components commute. Such an exercise provided enough confidence to proceed with deducing the turbulence measurements from the WindScanner using both methods.

4 Turbulence measurements

Two methods are used to deduce the turbulence statistics from the WindScanner measurements:

1. Six-Beam method – for each 30 min period the measured \mathbf{S} vector is used in combination with Eq. (5) to deduce the $\mathbf{\Sigma}$ vector. Finally the $\mathbf{\Sigma}$ vector is rotated in the mean wind direction for the respective 30 min period.
2. VAD method – within each 30 min period the v_r measurements from every single cycle of the six beams are fitted in a least squares sense to Eq. (2) to deduce

Six-beam method

A. Sathe et al.

Title Page

Abstract

Introduction

Conclusions

References

Tables

Figures

⏪

⏩

◀

▶

Back

Close

Full Screen / Esc

Printer-friendly Version

Interactive Discussion



a 30 min time series of the wind field components. The Σ vector is subsequently computed and rotated in the mean wind direction for the respective 30 min period.

Figure 5 shows the comparison of the turbulence statistics derived from the Wind-Scanner measurements using the six-beam and the VAD methods and those obtained from the cup anemometer under unstable conditions. It is clear that the six-beam method measures more turbulence, about 19% for $\langle u'^2 \rangle$ and 3% for $\langle v'^2 \rangle$ than the VAD method, where the orthogonal least-squares regression is used to fit the cup anemometer measurements. The scatter using both methods is comparable to each other, but there is a slightly more scatter using the six-beam method for $\langle v'^2 \rangle$.

Figure 6 shows the same as Fig. 5 but under neutral conditions. As for the unstable conditions, the six-beam method measures more turbulence, about 18% for $\langle u'^2 \rangle$ and 10% for $\langle v'^2 \rangle$ than the VAD method. The scatter using both methods is comparable to each other, with the six-beam method giving a slightly reduced scatter than the VAD method.

Figure 7 shows the same as Fig. 5 but under stable conditions. As for the unstable conditions, the six-beam method measures more turbulence, about 19% for $\langle u'^2 \rangle$ and 4% for $\langle v'^2 \rangle$ than the VAD method. The scatter using both methods is comparable to each other, but there is a slightly more scatter using the six-beam method for $\langle u'^2 \rangle$.

Thus under all stabilities the six-beam method is closer to the turbulence measurements carried out using the reference cup anemometer. There is however some probe volume averaging using both methods, but is significantly larger for the VAD method.

5 Discussion

From Figs. 5–7 it is clear that using both methods the WindScanner measures more turbulence under stable conditions than under unstable and neutral conditions. This may be contrary to our intuitive understanding, because usually the turbulence scales are much larger under unstable conditions than under stable conditions (Sathe et al.,

Six-beam method

A. Sathe et al.

Title Page

Abstract

Introduction

Conclusions

References

Tables

Figures



Back

Close

Full Screen / Esc

Printer-friendly Version

Interactive Discussion



Six-beam method

A. Sathe et al.

Title Page

Abstract

Introduction

Conclusions

References

Tables

Figures

◀

▶

◀

▶

Back

Close

Full Screen / Esc

Printer-friendly Version

Interactive Discussion



2013). These results are also contrary to what has been observed by Sathe et al. (2011b) at the same site. However, it is to be noted that Sathe et al. (2011b) used the lidar measurements when the wind was blowing from the eastern direction, whereas in this work we use the measurements when the wind is blowing from the western direction. As described in Sect. 4, in the western sector there is a sudden change of roughness due to the transition from sea to land. As a consequence there is a development of the internal boundary layer (IBL). Also the growth of the IBL depends on atmospheric stability, where under unstable conditions the growth will be faster than under stable conditions. Panofsky and Dutton (1984) state that the growth of the height of the boundary layer is proportional to the drag coefficient $u_* / \langle u \rangle$. And it is well known that the drag coefficient is larger for unstable stratification. Consequently the turbulence scales within the IBL will be smaller as compared to those outside of it. It is then interesting to check whether the WindScanner measures more within the IBL under unstable conditions as compared to the stable conditions.

Figure 8 shows the u and v spectra derived from high-frequency cup anemometer measurements under different stability conditions. If we define the characteristic length scale \mathcal{L} as the length scale corresponding to the maximum spectral energy, it is then clear that the peak of the v spectra is shifted to the right for unstable conditions as compared to the stable conditions. It is not that clear for the u spectra, however the shift of scales to larger wavenumbers under unstable conditions can still be observed. Thus \mathcal{L} appears smaller under unstable conditions than under stable conditions for the measurements from the western sector used in this work. There is thus more probe volume averaging under unstable conditions than under stable conditions. Hence the WindScanner attenuates the turbulence measurements lesser under unstable conditions than under stable conditions.

Another interesting observation is that using the VAD method the WindScanner does not measure more turbulence than the reference cup anemometer under any stability condition. This does not agree with that observed by Sathe et al. (2011b), even though the same basic pulsed commercial lidar technology was also used in that work. It is

sensitive to the turbulence structure in the atmosphere, and one must avoid using it to measure atmospheric turbulence.

Future studies must certainly focus on tackling the probe volume averaging effect, which will further strengthen the arguments of using the six-beam method. Smalikho et al. (2005) have provided us with such a framework for pulsed lidars, whereas Mann et al. (2010) have demonstrated it for a continuous-wave lidar.

Acknowledgements. This work is carried out as a part of a research project funded by the Danish Ministry of Science, Innovation and Higher Education – Technology and Production, grant no. 0602-02486B. The resources provided by the Center for Computational Wind Turbine Aerodynamics and Atmospheric Turbulence funded by the Danish Council for Strategic Research grant no. 09-067216 are also acknowledged. We also thank Erik Juul from DTU Wind Energy department for helping with some sketches.

References

- Banakh, V. A. and Smalikho, I. N.: Determination of the turbulent energy dissipation rate from lidar sensing data, *Atmospheric and Oceanic Optics*, 10, 295–302, 1997a. 10330
- Banakh, V. A. and Smalikho, I. N.: Estimation of the turbulence energy dissipation rate from the pulsed Doppler lidar data, *Atmospheric and Oceanic Optics*, 10, 957–965, 1997b. 10330
- Banakh, V. A. and Werner, C.: Computer simulation of coherent Doppler lidar measurement of wind velocity and retrieval of turbulent wind statistics, *Opt. Eng.*, 44, 071205, doi:10.1117/1.1955167, 2005. 10330
- Banakh, V. A., Smalikho, I. N., Köpp, F., and Werner, C.: Representativeness of wind measurements with a CW Doppler lidar in the atmospheric boundary layer, *Appl. Optics*, 34, 2055–2067, doi:10.1364/AO.34.002055, 1995a. 10330
- Banakh, V. A., Werner, C., Kerkis, N. N., Köpp, F., and Smalikho, I. N.: Turbulence measurements with a CW Doppler lidar in the atmospheric boundary layer, *Atmospheric and Oceanic Optics*, 8, 955–959, 1995b. 10330
- Banakh, V. A., Werner, C., Köpp, F., and Smalikho, I. N.: Measurement of turbulent energy dissipation rate with a scanning Doppler lidar, *Atmospheric and Oceanic Optics*, 9, 849–853, 1996. 10330

Six-beam method

A. Sathe et al.

Title Page

Abstract

Introduction

Conclusions

References

Tables

Figures



Back

Close

Full Screen / Esc

Printer-friendly Version

Interactive Discussion



Six-beam method

A. Sathe et al.

Title Page

Abstract

Introduction

Conclusions

References

Tables

Figures



Back

Close

Full Screen / Esc

Printer-friendly Version

Interactive Discussion



- Banakh, V. A., Smalikho, I. N., Köpp, F., and Werner, C.: Measurements of turbulent energy dissipation rate with a CW Doppler lidar in the atmospheric boundary layer, *J. Atmos. Ocean. Tech.*, 16, 1044–1061, doi:10.1175/1520-0426(1999)016<1044:MOTEDR>2.0.CO;2, 1999. 10330
- 5 Banakh, V. A., Smalikho, I. N., Pichugina, Y. L., and Brewer, W. A.: Representativeness of measurements of the dissipation rate of turbulence energy by scanning Doppler lidar, *Atmospheric and Oceanic Optics*, 23, 48–54, doi:10.1134/S1024856010010100, 2010. 10330
- Branlard, E., Pedersen, A. T., Mann, J., Angelou, N., Fischer, A., Mikkelsen, T., Harris, M., Slinger, C., and Montes, B. F.: Retrieving wind statistics from average spectrum of continuous-wave lidar, *Atmos. Meas. Tech.*, 6, 1673–1683, doi:10.5194/amt-6-1673-2013, 2013. 10330
- 10 Browning, K. A. and Wexler, R.: The determination of kinematic properties of a wind field using a Doppler radar, *J. Appl. Meteorol.*, 7, 105–113, doi:10.1175/1520-0450(1968)007<0105:TDOKPO>2.0.CO;2, 1968. 10329
- 15 Clifton, A., Elliott, D., and Courtney, M.: Ground-based vertically profiling remote sensing for wind resource assessment, Tech. Rep. 15, International Energy Agency, 2013. 10328
- Eberhard, W. L., Cupp, R. E., and Healy, K. R.: Doppler lidar measurements of profiles of turbulence and momentum flux, *J. Atmos. Ocean. Tech.*, 6, 809–819, doi:10.1175/1520-0426(1989)006<0809:DLMOPO>2.0.CO;2, 1989. 10329, 10330, 10331, 10332
- 20 Frehlich, R.: Coherent Doppler lidar signal covariance including wind shear and wind turbulence, *Appl. Optics*, 33, 6472–6481, doi:10.1364/AO.33.006472, 1994. 10330
- Frehlich, R.: Effects of wind turbulence on coherent Doppler lidar performance, *J. Atmos. Ocean. Tech.*, 14, 54–75, doi:10.1175/1520-0426(1997)014<0054:EOWTOC>2.0.CO;2, 1997. 10330
- 25 Frehlich, R. and Cornman, L.: Estimating spatial velocity statistics with coherent Doppler lidar, *J. Atmos. Ocean. Tech.*, 19, 355–366, doi:10.1175/1520-0426-19.3.355, 2002. 10330
- Frehlich, R. and Kelley, N.: Measurements of wind and turbulence profiles with scanning Doppler lidar for wind energy applications, *IEEE J. Sel. Top. Appl.*, 1, 42–47, doi:10.1109/JSTARS.2008.2001758, 2008. 10330
- 30 Frehlich, R., Hannon, S. M., and Henderson, S. W.: Performance of a 2- μ m coherent Doppler lidar for wind measurements, *J. Atmos. Ocean. Tech.*, 11, 1517–1528, doi:10.1175/1520-0426(1994)011<1517:POACDL>2.0.CO;2, 1994. 10330

Six-beam method

A. Sathe et al.

Title Page

Abstract

Introduction

Conclusions

References

Tables

Figures



Back

Close

Full Screen / Esc

Printer-friendly Version

Interactive Discussion



Frehlich, R., Hannon, S. M., and Henderson, S. W.: Coherent Doppler lidar measurements of wind field statistics, *Bound.-Lay. Meteorol.*, 86, 233–256, doi:10.1023/A:1000676021745, 1998. 10330

Frehlich, R., Meillier, Y., Jensen, M. L., Balsley, B., and Sharman, R.: Measurements of boundary layer profiles in urban environment, *J. Appl. Meteorol. Clim.*, 45, 821–837, doi:10.1175/JAM2368.1, 2006. 10330

Frehlich, R., Meillier, Y., and Jensen, M. L.: Measurements of boundary layer profiles with in situ sensors and Doppler lidar, *J. Atmos. Ocean. Tech.*, 25, 1328–1340, doi:10.1175/2007JTECHA963.1, 2008. 10330

Gal-Chen, T., Xu, M., and Eberhard, W. L.: Estimation of atmospheric boundary layer fluxes and other turbulence parameters from Doppler lidar data, *J. Geophys. Res.*, 97, 18409–18423, doi:10.1029/91JD03174, 1992. 10330

Ingber, L.: Simulated annealing: practice versus theory, *Math. Comput. Model.*, 18, 29–57, 1993. 10338

Kaimal, J. C. and Finnigan, J. J.: Acquisition and processing of atmospheric boundary layer data, in: *Atmospheric Boundary Layer Flows – Their Structure and Measurement*, Oxford University Press, New York, 254–281, 7, 1994. 10340

Kindler, D., Oldroyd, A., Macaskill, A., and Finch, D.: An eight month test campaign of the QinetiQ ZephIR system: preliminary results, *Meteorol. Z.*, 16, 479–489, doi:10.1127/0941-2948/2007/0226, 2007. 10328

Kropfli, R. A.: Single Doppler radar measurement of turbulence profiles in the convective boundary layer, *J. Atmos. Ocean. Tech.*, 3, 305–314, doi:10.1175/1520-0426(1986)003<0305:SDRMOT>2.0.CO;2, 1986. 10329, 10330, 10331

Lenschow, D. H., Mann, J., and Kristensen, L.: How long is long enough when measuring fluxes and other turbulence statistics?, *J. Atmos. Ocean. Tech.*, 11, 661–673, doi:10.1175/1520-0426(1994)011<0661:HLILEW>2.0.CO;2, 1994. 10340

Lhermitte, R. M.: Note on wind variability with Doppler radar, *J. Atmos. Sci.*, 19, 343–346, doi:10.1175/1520-0469(1962)019<0343:NOWVWD>2.0.CO;2, 1962. 10329

Lhermitte, R. M.: Note on the observation of small-scale atmospheric turbulence by Doppler radar techniques, *Radio Sci.*, 4, 1241–1246, doi:10.1029/RS004i012p01241, 1969. 10329, 10331, 10332

Mann, J., Cariou, J., Courtney, M., Parmentier, R., Mikkelsen, T., Wagner, R., Lindelow, P., Sjöholm, M., and Enevoldsen, K.: Comparison of 3D turbulence measurements using three

Six-beam method

A. Sathe et al.

Title Page

Abstract

Introduction

Conclusions

References

Tables

Figures

◀

▶

◀

▶

Back

Close

Full Screen / Esc

Printer-friendly Version

Interactive Discussion



staring wind lidars and a sonic anemometer, *Meteorol. Z.*, 18, 135–140, doi:10.1127/0941-2948/2009/0370, 2009. 10330

Mann, J., Peña, A., Bingöl, F., Wagner, R., and Courtney, M. S.: Lidar scanning of momentum flux in and above the surface layer, *J. Atmos. Ocean. Tech.*, 27, 792–806, doi:10.1175/2010JTECHA1389.1, 2010. 10329, 10330, 10331, 10345

Nelder, J. A. and Mead, R.: A simplex method for function minimization, *Comput. J.*, 7, 308–313, 1965. 10338

Panofsky, H. A. and Dutton, J. A.: *Atmospheric Turbulence*, John Wiley and Sons, New York, 1984. 10343

Peña, A., Hasager, C. B., Gryning, S.-E., Courtney, M., Antoniou, I., and Mikkelsen, T.: Offshore wind profiling using light detection and ranging measurements, *Wind Energy*, 12, 105–124, doi:10.1002/we.283, 2009. 10328

Rao, S.: *Engineering Optimization: Theory and Practice*, 4th Edn., John Wiley and Sons Inc., Hoboken, New Jersey, 2009. 10338

Sathe, A. and Mann, J.: Measurement of turbulence spectra using scanning pulsed wind lidars, *J. Geophys. Res.*, 117, D01201, doi:10.1029/2011JD016786, 2012. 10329, 10330

Sathe, A. and Mann, J.: A review of turbulence measurements using ground-based wind lidars, *Atmos. Meas. Tech.*, 6, 3147–3167, doi:10.5194/amt-6-3147-2013, 2013. 10330

Sathe, A., Gryning, S.-E., and Peña, A.: Comparison of the atmospheric stability and wind profiles at two wind farm sites over a long marine fetch in the North Sea, *Wind Energy*, 14, 767–780, doi:10.1002/we.456, 2011a. 10340

Sathe, A., Mann, J., Gottschall, J., and Courtney, M. S.: Can wind lidars measure turbulence?, *J. Atmos. Ocean. Tech.*, 28, 853–868, doi:10.1175/JTECH-D-10-05004.1, 2011b. 10328, 10329, 10330, 10331, 10343, 10344

Sathe, A., Mann, J., Barlas, T., Bierbooms, W. A. A. M., and van Bussel, G. J. W.: Influence of atmospheric stability on wind turbine loads, *Wind Energy*, 16, 1013–1032, doi:10.1002/we.1528, 2013. 10342

Sjöholm, M., Mikkelsen, T., Mann, J., Enevoldsen, K., and Courtney, M.: Spatial averaging-effects on turbulence measured by a continuous-wave coherent lidar, *Meteorol. Z.*, 18, 281–287, doi:10.1127/0941-2948/2009/0379, 2009. 10330

Smalikho, I. N.: On measurement of dissipation rate of the turbulent energy with a CW Doppler lidar, *Atmospheric and Oceanic Optics*, 8, 788–793, 1995. 10330

Six-beam method

A. Sathe et al.

Title Page

Abstract

Introduction

Conclusions

References

Tables

Figures



Back

Close

Full Screen / Esc

Printer-friendly Version

Interactive Discussion



Smalikho, I., Kopp, F., and Rahm, S.: Measurement of atmospheric turbulence by 2- μm Doppler lidar, *J. Atmos. Ocean. Tech.*, 22, 1733–1747, doi:10.1175/JTECH1815.1, 2005. 10330, 10345

Smith, D. A., Harris, M., Coffey, A. S., Mikkelsen, T., Jørgensen, H. E., Mann, J., and Danielian, R.: Wind lidar evaluation at the danish wind test site in Høvsøre, *Wind Energy*, 9, 87–93, doi:10.1002/we.193, 2006. 10328

Vasiljevic, N.: A time-space synchronization of coherent Doppler scanning lidars for 3D measurements of wind fields, Ph.D. Thesis PhD-0027 (EN), Technical University of Denmark, 2014. 10339

Wagner, R., Courtney, M., Gottschall, J., and Lindelöw-Marsden, P.: Accounting for the speed shear in wind turbine power performance measurement, *Wind Energy*, 14, 993–1004, doi:10.1002/we.509, 2011. 10328

Wilson, D. A.: Doppler radar studies of boundary layer wind profiles and turbulence in snow conditions, in: *Proc. 14th Conference on Radar Meteorology*, Tucson, USA, 191–196, 1970. 10329, 10330, 10331

Six-beam method

A. Sathe et al.

Title Page

Abstract

Introduction

Conclusions

References

Tables

Figures



Back

Close

Full Screen / Esc

Printer-friendly Version

Interactive Discussion

**Table 1.** Optimum six-beam configuration.

Beam no.	1	2	3	4	5	6
θ°	0	72	144	216	288	288
ϕ°	45	45	45	45	45	0

Six-beam method

A. Sathe et al.

Title Page

Abstract

Introduction

Conclusions

References

Tables

Figures

◀

▶

◀

▶

Back

Close

Full Screen / Esc

Printer-friendly Version

Interactive Discussion

**Table 2.** Classification of atmospheric stability according to Monin–Obukhov length intervals.

unstable (u)	$-500 \leq L_{MO} \leq -50 \text{ m}$
neutral (n)	$ L_{MO} \geq 500 \text{ m}$
stable (s)	$10 \leq L_{MO} \leq 500 \text{ m}$

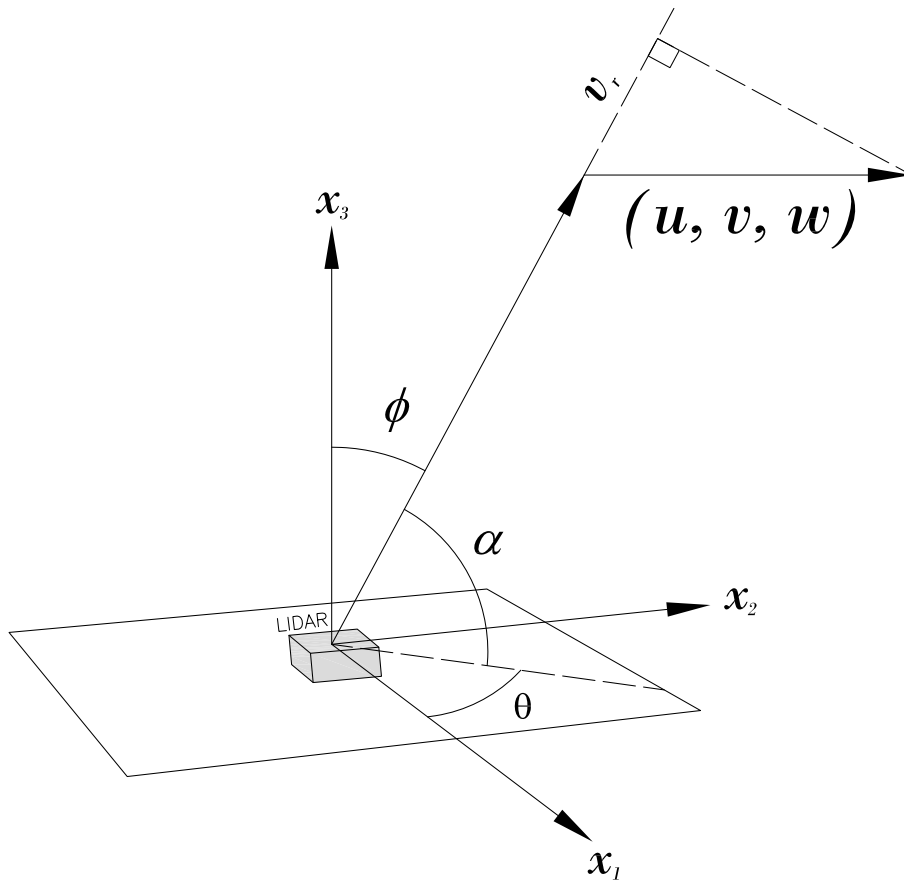


Figure 1. Coordinate system of a lidar.

Six-beam method

A. Sathe et al.

Title Page

Abstract

Introduction

Conclusions

References

Tables

Figures

◀

▶

◀

▶

Back

Close

Full Screen / Esc

Printer-friendly Version

Interactive Discussion



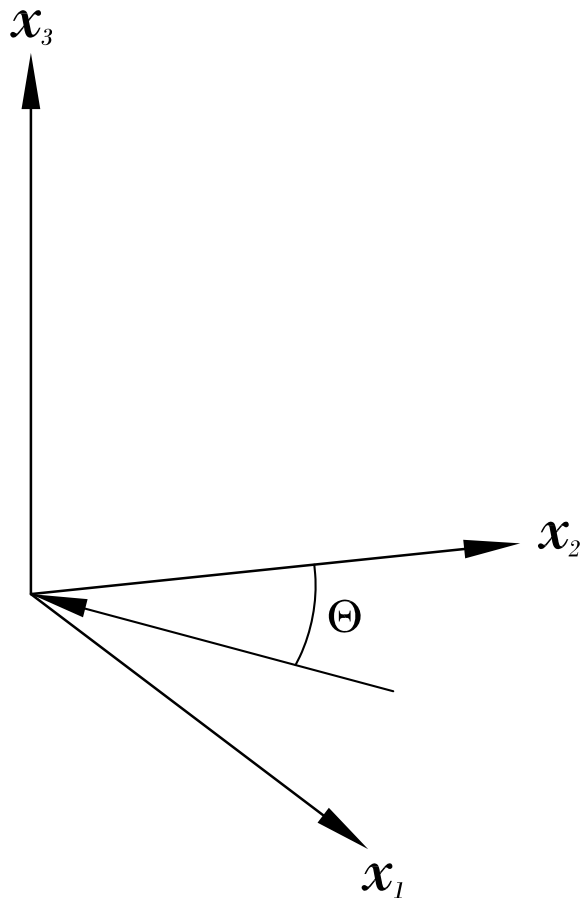


Figure 2. Standard meteorological convention of depicting the mean wind direction.

Six-beam method

A. Sathe et al.

Title Page

Abstract

Introduction

Conclusions

References

Tables

Figures



Back

Close

Full Screen / Esc

Printer-friendly Version

Interactive Discussion



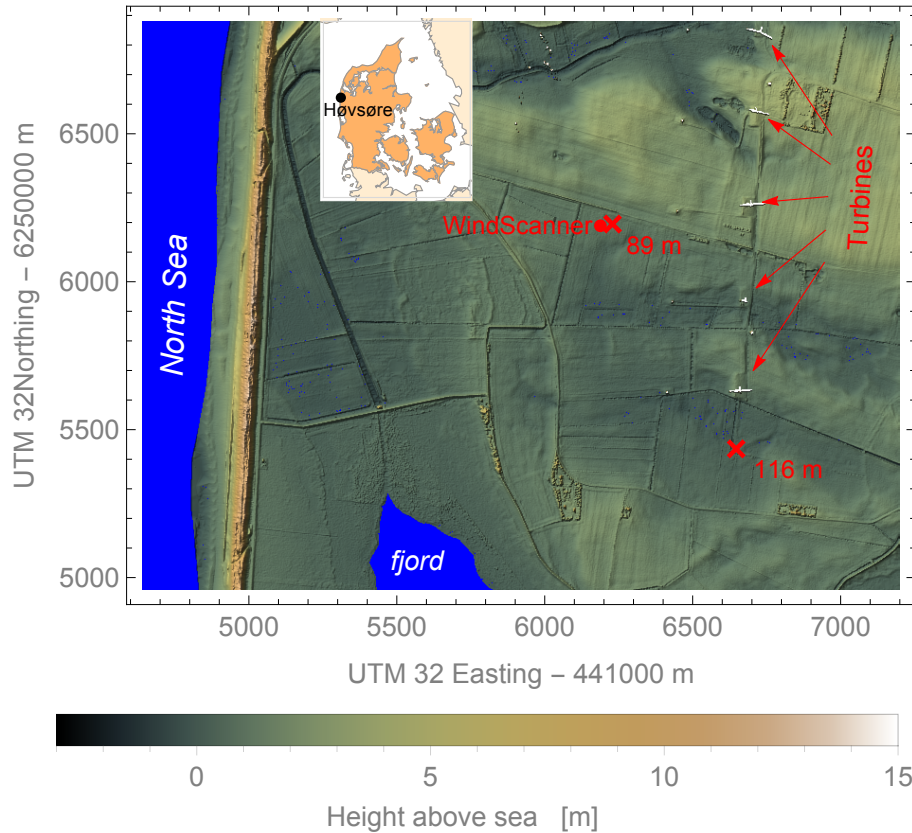


Figure 3. Location of the Høvsøre test center in Denmark (inset) and details of the site, where the location of the WindScanner and the met masts are shown.

Title Page

Abstract

Introduction

Conclusions

References

Tables

Figures

◀

▶

◀

▶

Back

Close

Full Screen / Esc

Printer-friendly Version

Interactive Discussion



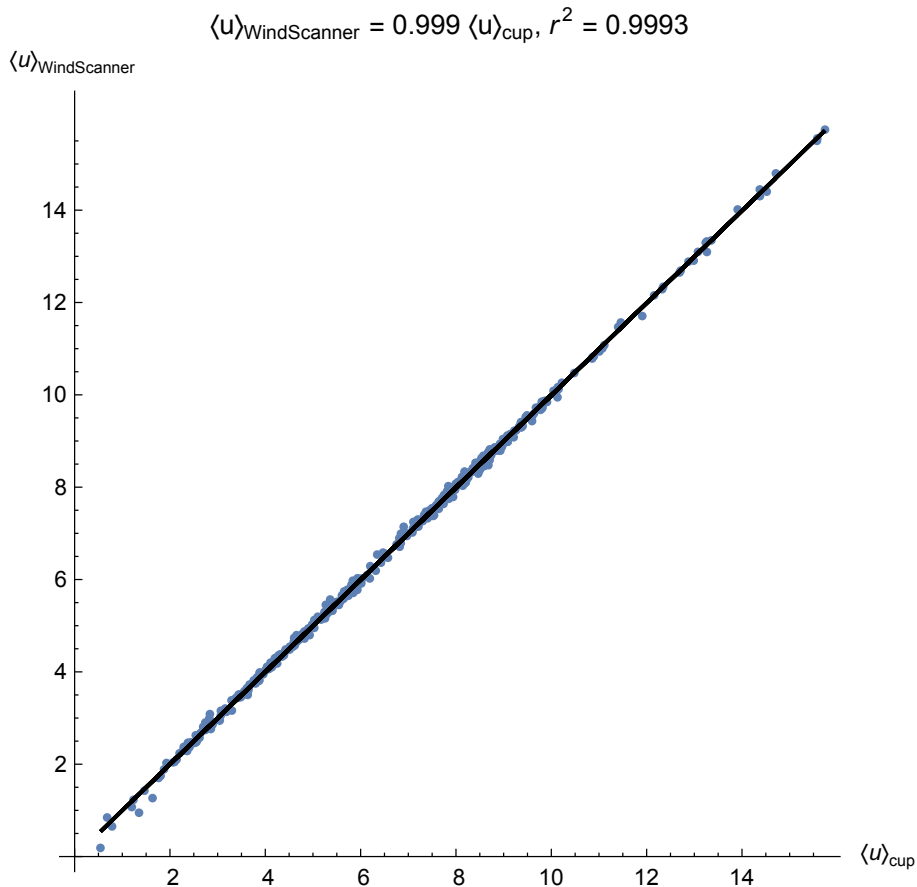


Figure 4. Comparison of the 30 min mean wind speed between the WindScanner and a cup anemometer using two methods.

Six-beam method

A. Sathe et al.

Title Page	
Abstract	Introduction
Conclusions	References
Tables	Figures
◀	▶
◀	▶
Back	Close
Full Screen / Esc	
Printer-friendly Version	
Interactive Discussion	



Six-beam method

A. Sathe et al.

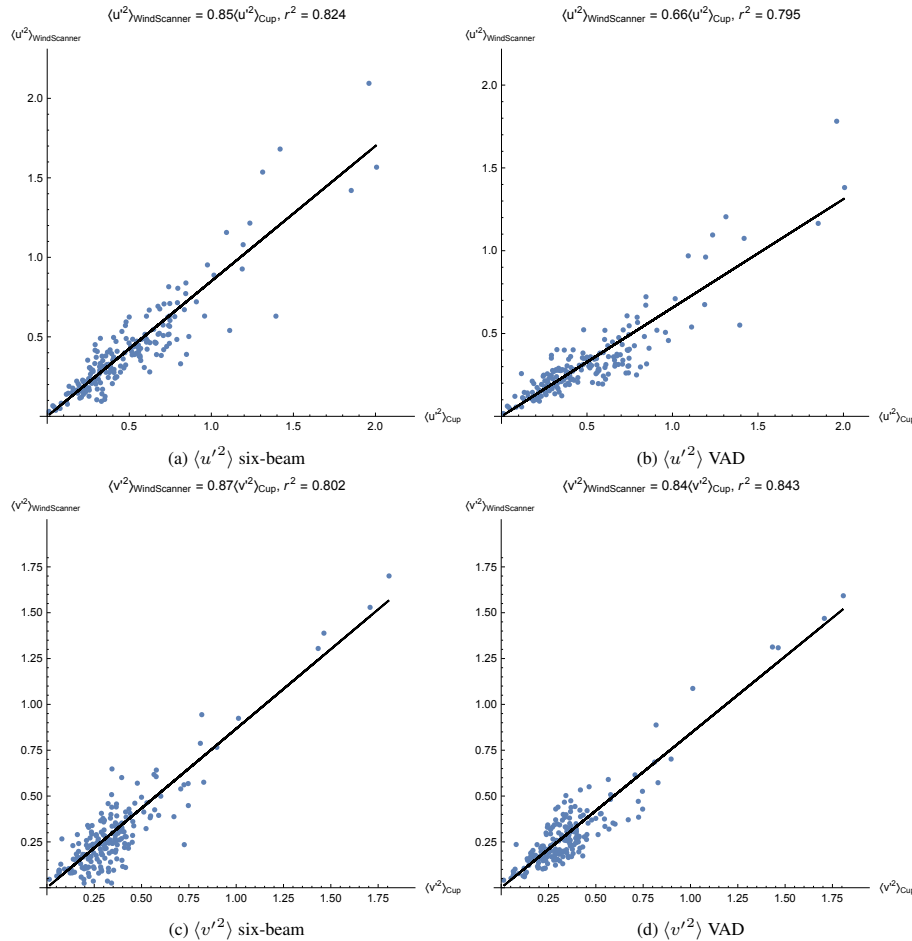


Figure 5. Comparison of the the turbulence statistics under unstable conditions between the WindScanner and the cup anemometer using two methods.

Title Page	
Abstract	Introduction
Conclusions	References
Tables	Figures
◀	▶
◀	▶
Back	Close
Full Screen / Esc	
Printer-friendly Version	
Interactive Discussion	



Six-beam method

A. Sathe et al.

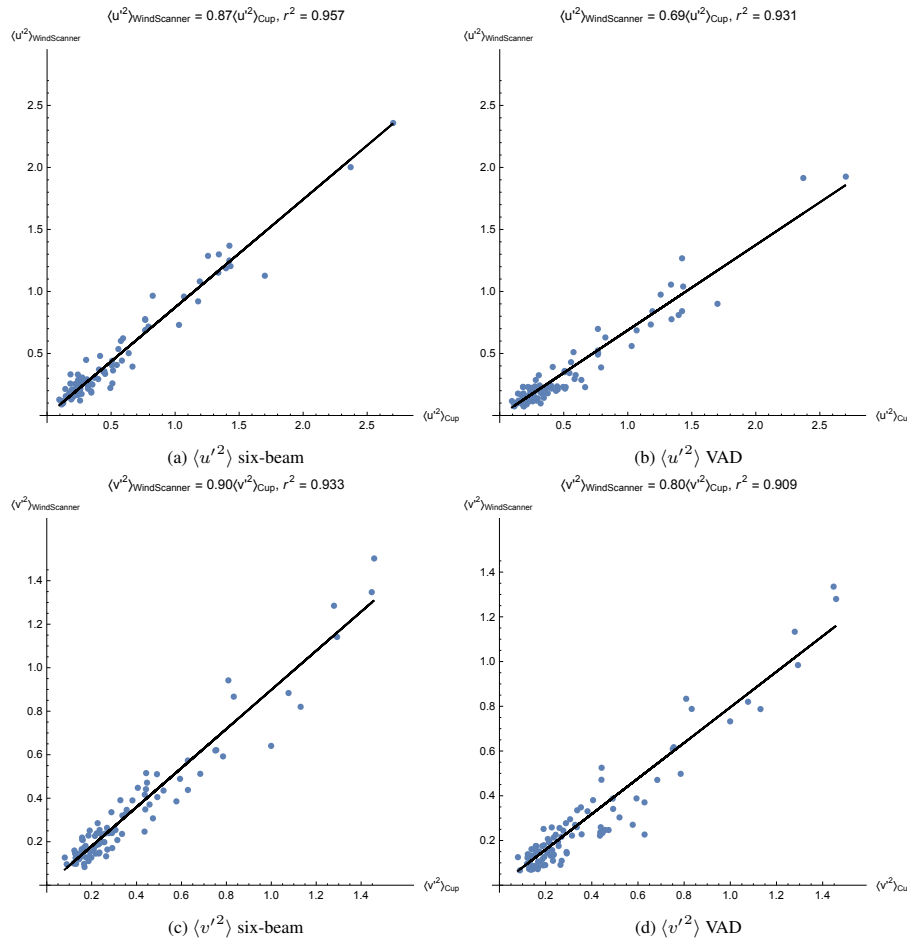


Figure 6. Comparison of the the turbulence statistics under neutral conditions between the WindScanner and the cup anemometer using two methods.

Title Page	
Abstract	Introduction
Conclusions	References
Tables	Figures
◀	▶
◀	▶
Back	Close
Full Screen / Esc	
Printer-friendly Version	
Interactive Discussion	



Six-beam method

A. Sathe et al.

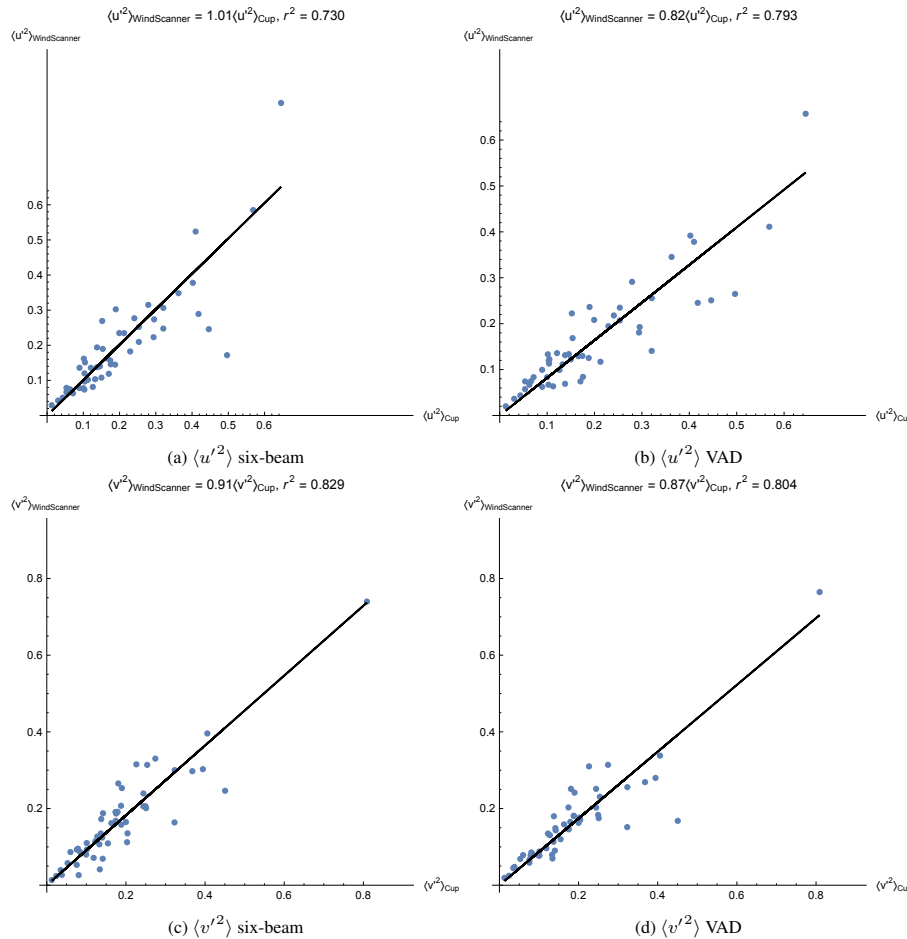


Figure 7. Comparison of the the turbulence statistics under stable conditions between the WindScanner and the cup anemometer using two methods.

Title Page	
Abstract	Introduction
Conclusions	References
Tables	Figures
◀	▶
◀	▶
Back	Close
Full Screen / Esc	
Printer-friendly Version	
Interactive Discussion	



